6.8.3 Blanket - The approach for developing the Prometheus blanket design was strongly based on considerations of safety, reliability, simplicity, and flexibility. Safety considerations led to the choice of a helium-cooled, solid-breeder blanket with low activation materials—SiC structure and neutron reflector and Li_2O breeder. Use of Li_2O in conjunction with the first wall Pb coolant provided the potential for adequate tritium breeding without the need for Be as a multiplier. Considerations of simplicity and design flexibility led to a well-studied, multi-layered, modular configuration similar to that used in the ARIES study,[1] which uses assumptions consistent with those of the present study. This design approach was adapted with minor modifications to both the laser and heavy ion reactor concepts.

6.8.3.1 Configuration - The blanket configuration consists of modular rings stacked around the cavity chamber. Each ring contains a number of modules placed circumferentially next to each other. At each beam penetration hole, the corresponding module length is shortened or the module side wall is curved to allow for penetration space. This is the major difference between the laser and heavy ion concepts, the former requiring allowances for 60 beam penetrations whereas the latter requires allowances for only 2 small beam penetrations, thereby resulting in simpler module design and assembly. Vacuum penetrations are required on both designs. A blanket module schematic is shown in Figure 6.8.3-1. It consists of a simple layered configuration of SiC. The module contains a number of U-bend woven SiC tube sheets which contain the pressurized flowing He coolant. The Li_2O is in a packed bed formed between the tube sheets and is purged by He flowing through the U-bend Li_2O regions.

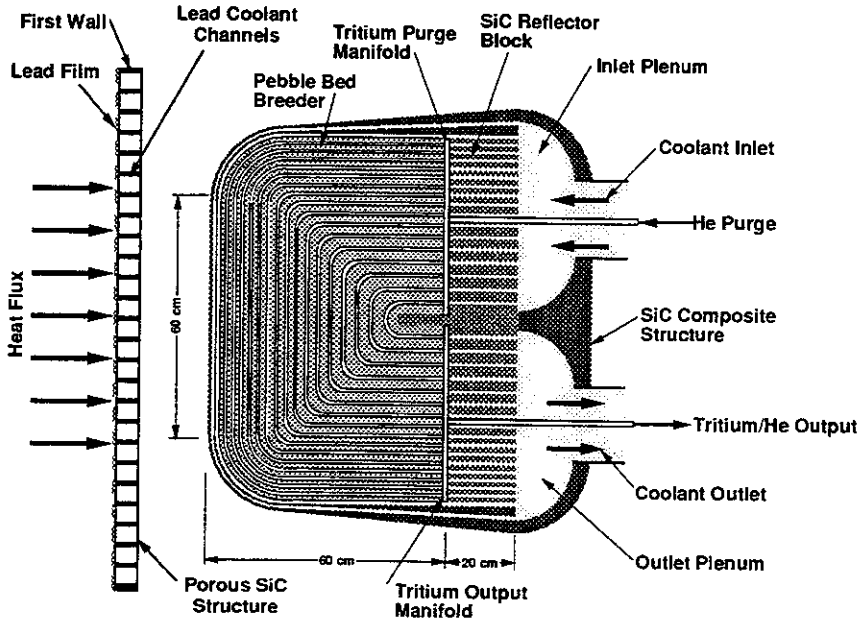

Figure 6.8.3-1. Schematic of a Blanket Module

Figure 6.8.3-2 shows an enlarged cutaway of the breeder region indicated in Figure 6.8.3-1. The SiC tube sheets on each side of the breeder region are 1-cm thick. The breeder region thickness increases with the distance from the plasma based on the local heat generation and minimum and maximum Li_2O operating temperature limits. These limits were conservatively set at 400°C and 800°C based on considerations of LiOT precipitation and sintering, respectively. For comparison, the corresponding temperature limits assumed in the ITER design study were 320°C and 1000°C, respectively.[2]

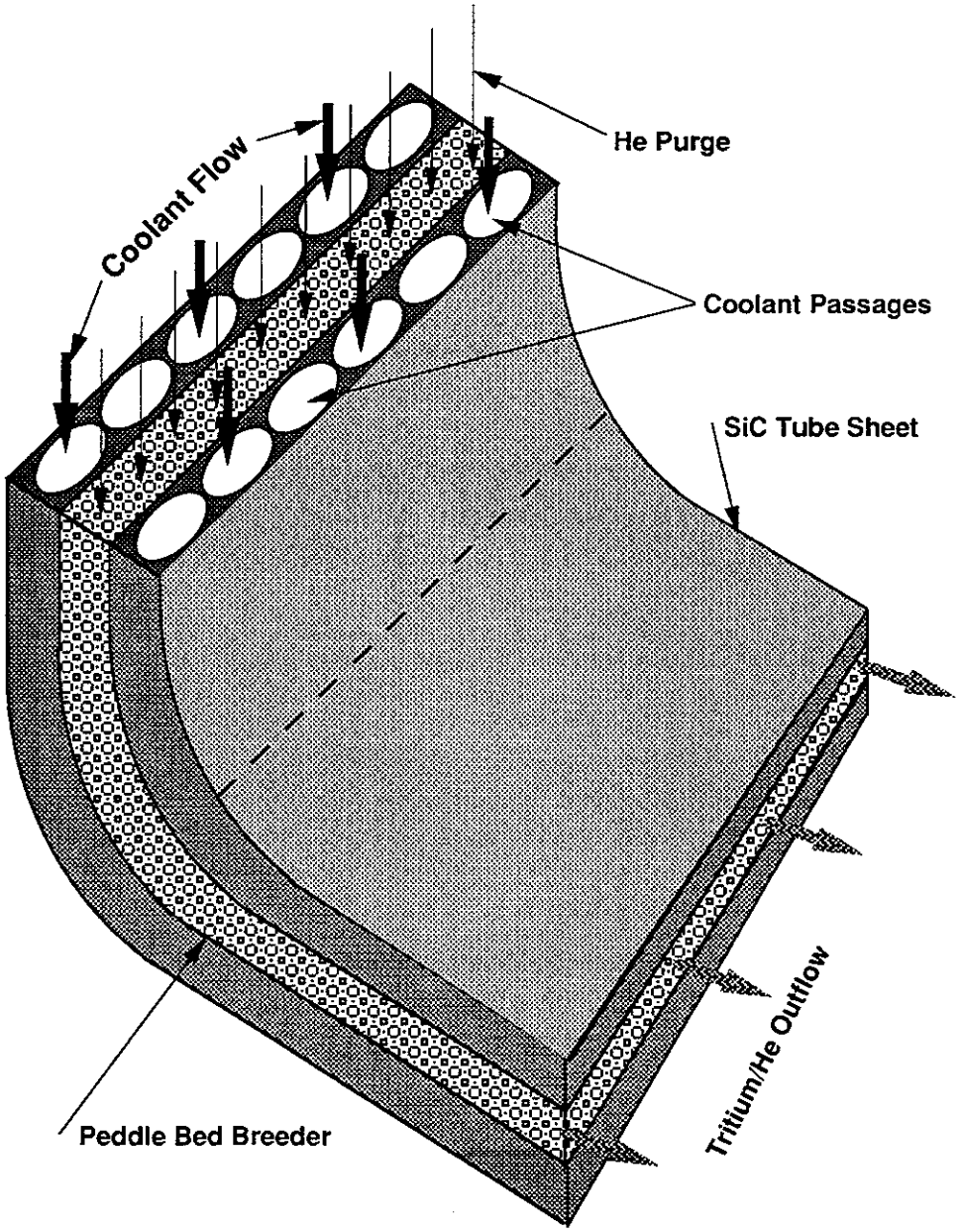

Figure 6.8.3-2. Enlarged Breeder Region Cutaway

Figure 6.8.3-3 shows the internal structure of a blanket module, including the coolant and purge manifolds. Reinforcing ribs are placed about every 25 cm along the module axis in order for the module to withstand the coolant pressure in case of failure of the coolant tubes. This effectively provides double containment of the coolant, thereby increasing the safety and reliability of the design.

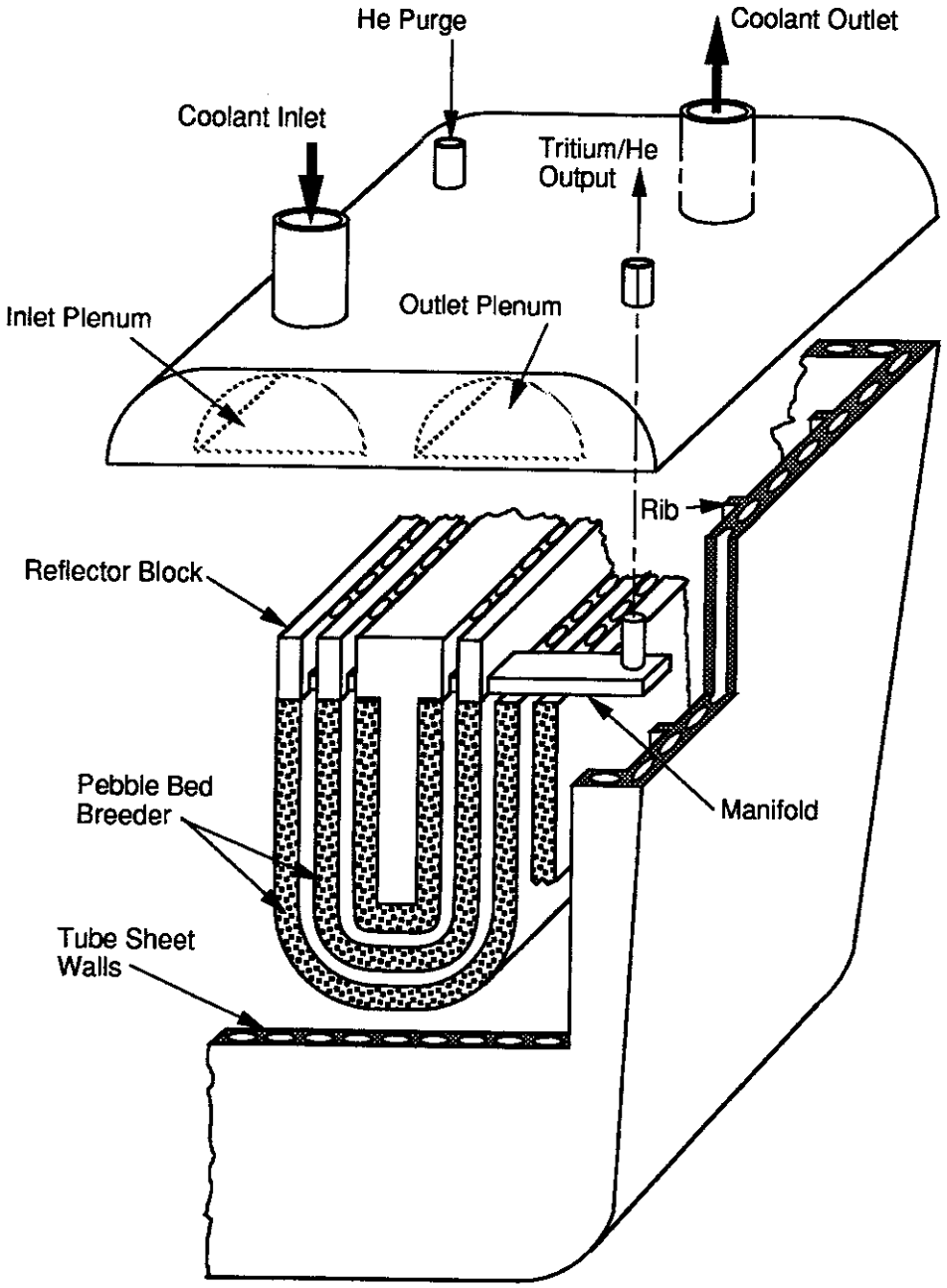

Figure 6.8.3-3. Blanket Module Internal Structure Showing Coolant and Purge Manifolds and Reinforcing Ribs

The final blanket performance parameters are summarized in Table 6.8.3-1 for both the laser and heavy ion reactor concepts. The main difference between the two concepts is small differences in the fusion and blanket power capacities. The design calculations and analyses in the key areas of neutronics, thermal-hydraulic, thermomechanics, tritium inventory, and tritium permeation are described in Sections 6.8.3.2 to 6.8.3.5.

Table 6.8.3-1 Final Blanket Performance Parameters

	Laser	Heavy Ion
Blanket Loop Power	1782 MW	1597 MW
Helium Inlet Temperature	400°C	400°C
Helium Outlet Temperature	650°C	650°C
Helium Inlet Pressure	1.5 MPa	1.5 MPa
Helium Velocity	46 m/s	42 m/s
Pressure Drop	24 kPa	19 kPa
Li_2O Min. Temperature	425°C	422°C
Li_2O Max. Temperature	800°C	765°C
Breeder Volume	92 m^3	75 m^3
Avg. Annual Li Burnup	0.5%	0.6%
Peak-to-Avg. Burnup	3	3
Tritium Breeding Ratio	1.2	1.2
Tritium Inventory	100 g	100 g
Purge Composition	He+0.2%H_2	He+0.2%H_2
Purge Pressure	1 MPa	1 MPa
SiC Min. Temperature	400°C	400°C
SiC Max. Temperature	800°C	765°C

6.8.3.2 Blanket Neutronics - Several neutronics calculations have been performed to arrive at the baseline design for the first wall/blanket/shield configuration. The objectives have been to maximize both the cavity power multiplication factor, M, and tritium breeding ratio, TBR. The incident neutron spectrum of the SIRIUS-M [3] reactor design was used as the representative neutron source resulting from the blast. About 78% of the target neutrons are 14.1 MeV neutrons, 21% are in the energy range 3.5-14.1 MeV, and ~1% are in the energy range 1.5–3.5 MeV. Thus, the average energy of the incident neutrons is ~12.87 MeV. No gamma-rays were considered. In addition, no time-dependent calculations were performed to calculate the instantaneous heating or damage rates in the first wall/blanket system due to

The module assembly is constructed by positioning the SiC woven U-tubes in the module box. The breeder regions between the coolant tubes are then packed with the Li_2O particles, starting with the larger size. The purge manifolds are then positioned, followed by the solid SiC block reflector region. Finally, the module top cover is assembled.

differences in the arrival time of neutrons to the first wall. Thus, the results reported here are the time-averaged values for the key parameters such as blanket power multiplication and tritium breeding ratio.

As discussed in Section 6.8.1, the incident neutron power in the laser reactor design is ~2027 MW and ~1818 MW in the heavy ion reactor (see Table 6.8.1-3). For an average neutron energy of 12.87 MeV, the incident neutron source is estimated to be ~9.83 x 10^{20} n/sec and 8.82 x 10^{20} n/sec in the two reactors, respectively.

One-dimensional and spherical model calculations were performed by using the ANISN 1-D discrete ordinate transport code[4] along with the the MATXS5 (30-g neutrons, 21-g) library[5] based on ENDF/B-V nuclear data. The 1-D model used is shown in Figure 6.8.3-4 for the final baseline design which was evolved from the parametric study given below. The material volume fractions used in the calculations are shown in Figure 6.8.3-5. The model considered a manifold zone of thickness ~1.8 m and a 1.48-m thick maintenance gap behind the vacuum vessel (2-cm thick). SiC has been selected as the structural material in the first wall and blanket/reflector/plena systems. It was also chosen as the reflecting material in the reflector/plena regions (40-cm thick) due to the high neutron reflectivity property of carbon. SiC has lower absorption cross-section for neutrons when compared to stainless steels. This choice is advantageous as far as tritium breeding is concerned because a lower absorption rate in the structural material leads to a higher absorption rate in the breeding material. However, power multiplication in steels are normally larger than in the SiC structure due to the larger energy release from the (n,γ) reactions in steels.

In the parametric study performed, a stainless steel-reinforced concrete (87% concrete, 8% carbon-steel, and 5% water) was considered for the bulk shield behind the vacuum vessel, although a composite shielding material consisting of 20% Pb, 20% B_4C, 25% SiC, 30% water, and 5% aluminum was adopted in the baseline design. Note that the bulk shield thickness in the calculational model shown in Figure 6.8.3-4 is 210 cm thick. In the final design, a thinner shield was adopted (165-cm thick in the concrete bulk shield case, 130-cm thick in the composite bulk shield case). The criterion used in estimating the required bulk shield thickness behind the vacuum vessel is discussed in Section 6.8.1 and in Section 6.8.4. It was shown that the tritium breeding ratio and cavity power multiplication are less sensitive to an increase in the bulk shield thickness beyond 1 m.

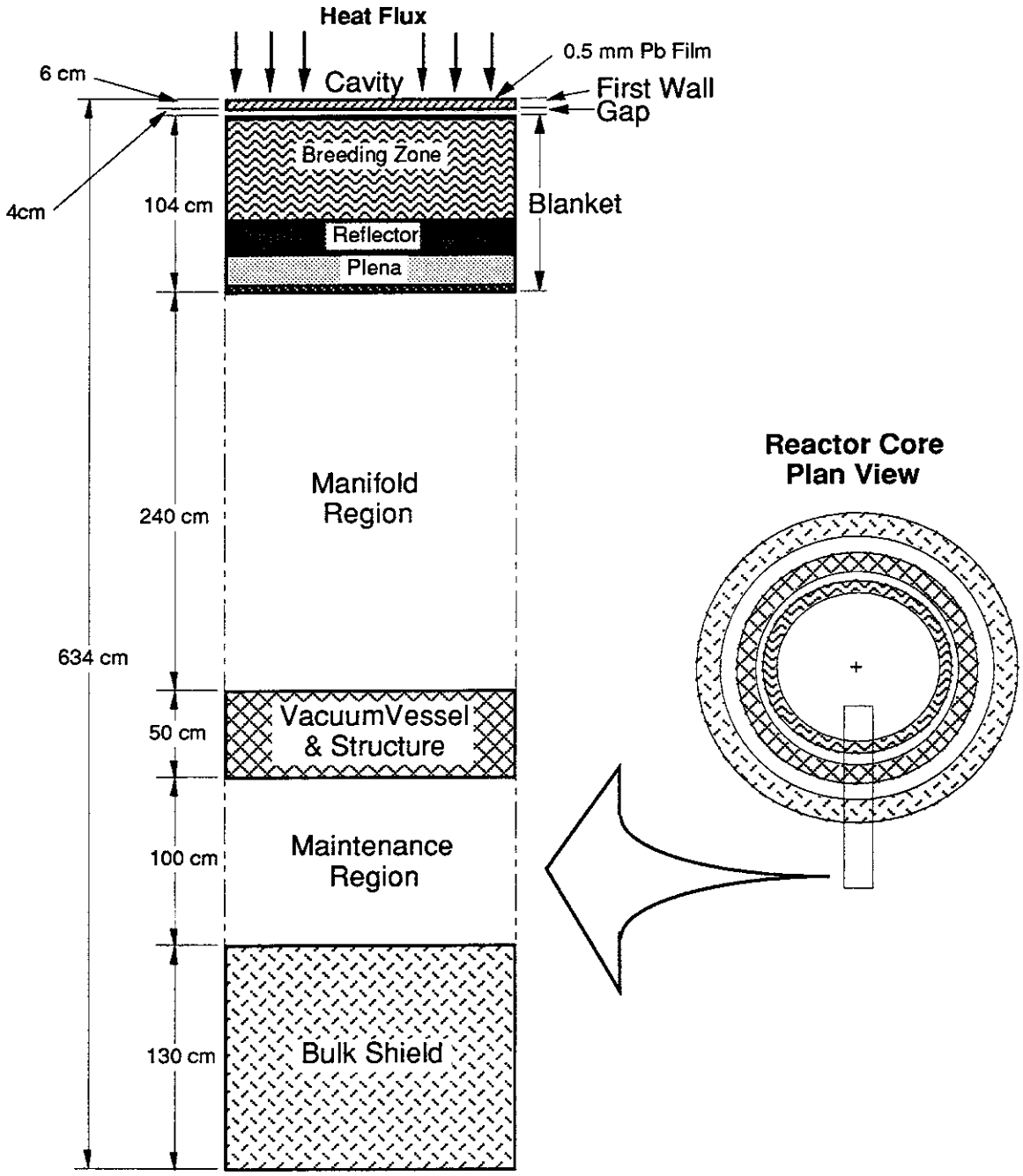

Figure 6.8.3-4. The Radial-Build of the Prometheus Cavity

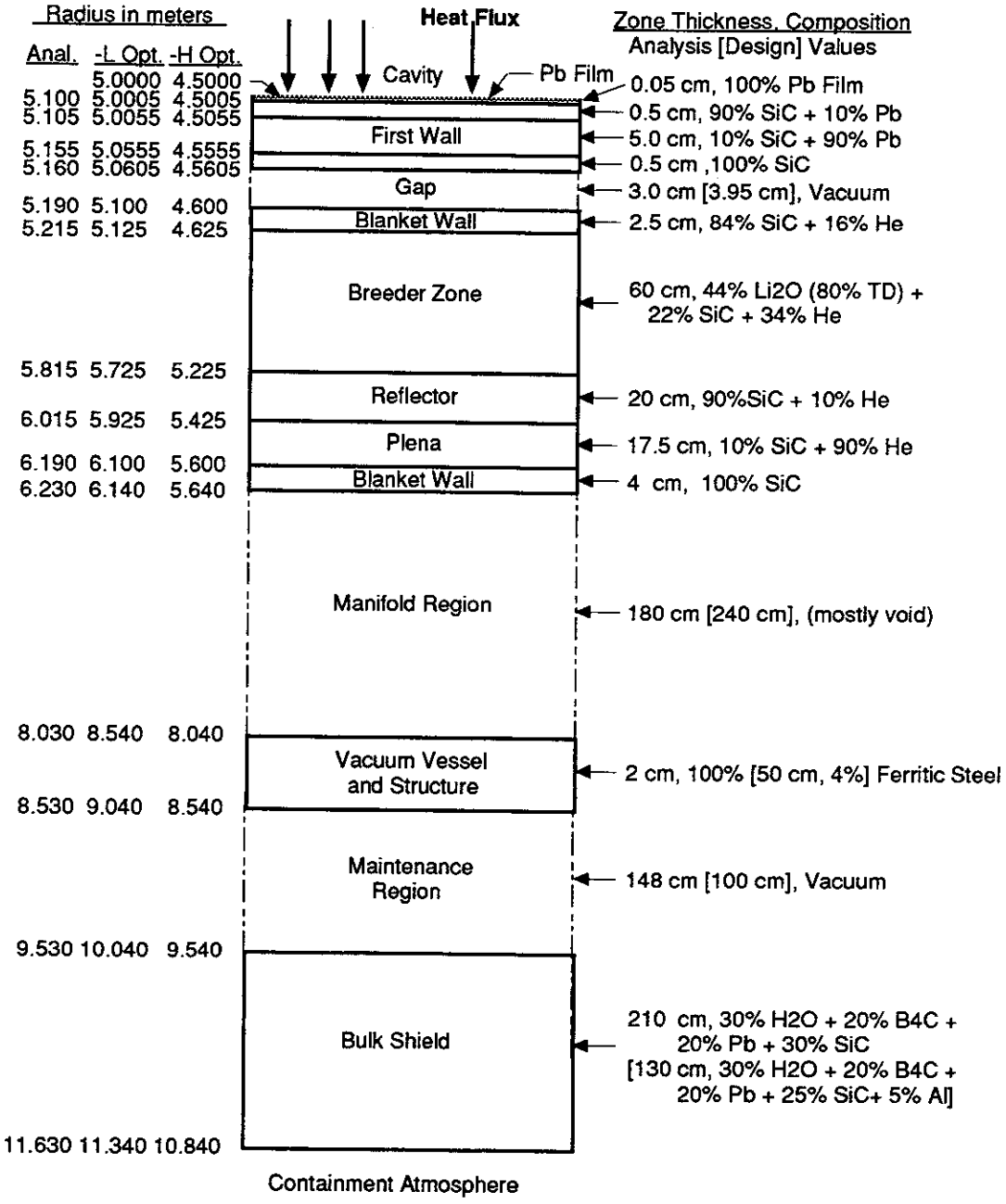

Figure 6.8.3-5. Material Composition in the 1-D Cavity Model

Geometry Normalization - The first wall in the analytical model shown in Figure 6.8.3-4 and Figure 6.8.3-5 is placed at a radial distance of 510 cm from the cavity center. The cavity radius in the final laser reactor design is 500 cm and, thus, a normalization factor of $(510/500)^2 \sim 1.04$ should be applied to local absolute values such as the local heating rate profiles. The cavity radius in the heavy ion reactor design is 450 cm. Considering the slight difference in the neutron source strength between the two reactors, the normalization factor to be applied to local absolute values in this case is $(510/450)^2 \cdot (8.82/9.83) \sim 1.15$.

Effect of Design Variation on Tritium Breeding Ratio and Cavity Power Multiplication - Factors varied in the parametric analysis performed were the ^{6}Li-enrichment, the diameter of the lead cooling channels in the first wall system (FWS), and the thickness of the breeding zone (X_B) in the blanket/reflector/plena system (B/R/P) (see Figure 6.8.3-4). In the first wall system, lead flows through near-rectangular channels in the zone between the first wall (0.5 cm-thick, 90% SiC, 10% Pb) and the back wall of the first wall system (0.5 cm-thick, 100% SiC). The volume fraction of the SiC and lead was kept to 9:1 in this zone whose thickness, denoted Xp, was varied in the present study.

For a total thickness of 104 cm for the B/R/P system, while keeping the thicknesses of other zones shown in Figure 6.8.3-5 the same, the power multiplication factor M has increased from 1.096 to 1.152 (~5% increase) for increasing X_p from 1 cm to 7 cm (see Figure 6.8.3-6). For the same change, the TBR [dominated by tritium production from ^{6}Li (T-6), 25% ^{6}Li-enrichment] has increased from 0.98 to 1.28; i.e., ~30% increase (see Figure 6.8.3-7). The fraction of nuclear power deposited in the first wall system is appreciable due to the interaction of neutrons and gamma rays with lead. This fraction increased from ~0.1 to ~0.25 for increasing X_p from 1 cm to 7 cm. The balance of the nuclear power is deposited mainly in the B/R/P system. This can be seen in Figures 6.8.3-8 and 6.8.3-9 which give the fraction of power deposited in the various components of the cavity. Note, in particular, the small fraction of power deposited in the vacuum vessel and shield systems .

The profiles for the nuclear power density (heating rate) as a function of the lead zone thickness, Xp, are shown in Figures 6.8.3-10 and 6.8.3-11 in units of J/cc.sec.n and in MW/m^3, respectively. For an Xp value of 1 cm, the power density in the lead and the back wall of the FWS is as high as 45 MW/m^3, while it is ~28 MW/m^3 in the first wall (see Figure 6.8.3-11). The power density in the lead film (0.05 cm-thick) covering the inner surface of the cavity is ~42 MW/m^3 in this case. As Xp increases, the power density in the first wall system decreases rapidly, while the power deposited in the blanket/reflector/plena system increases. For the baseline design (Xp = 5 cm), the power density in the lead film is ~32 MW/m^3 and mainly due to gamma rays produced

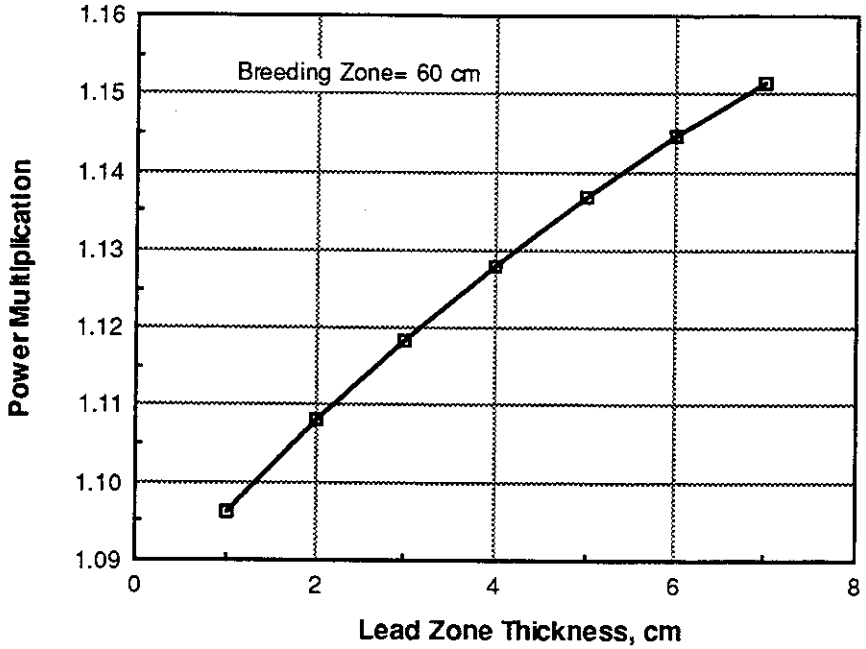

Figure 6.8.3-6. Nuclear Power Multiplication as a Function of Lead Zone Thickness

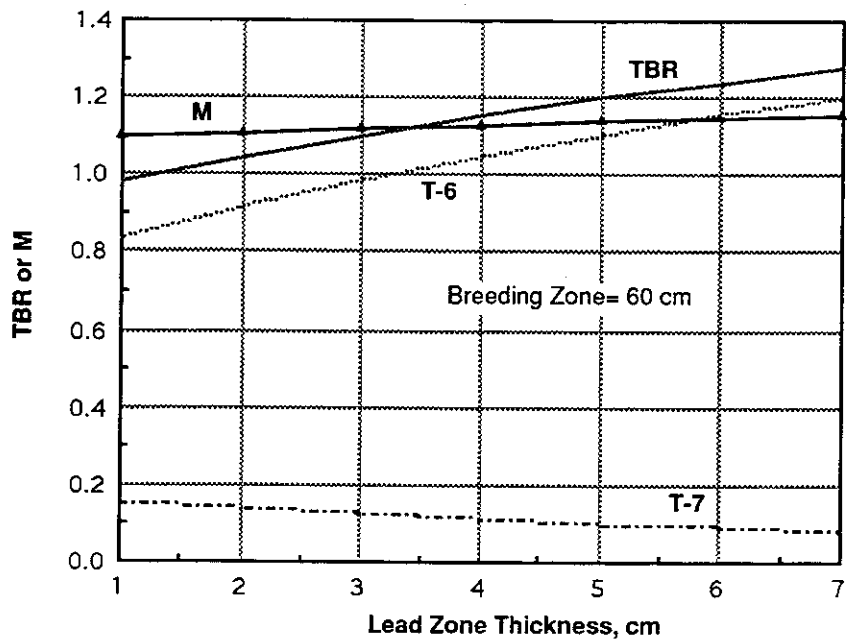

Figure 6.8.3-7. Tritium Breeding Ratio and Nuclear Power Multiplication as a Function of Lead Zone Thickness

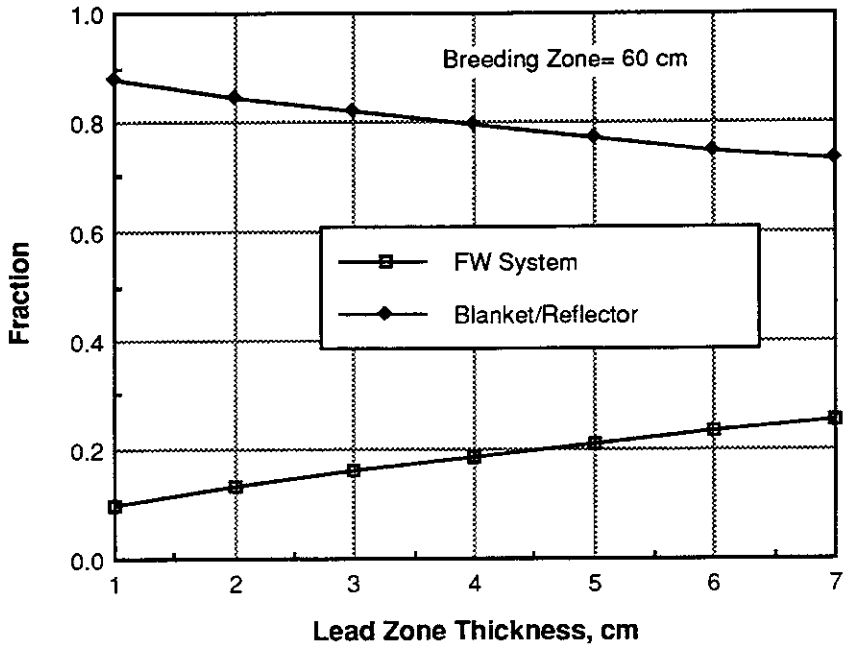

Figure 6.8.3-8. Fraction of Nuclear Power Deposited in the First Wall and Blanket/Reflector Systems as a Function of Lead Zone Thickness

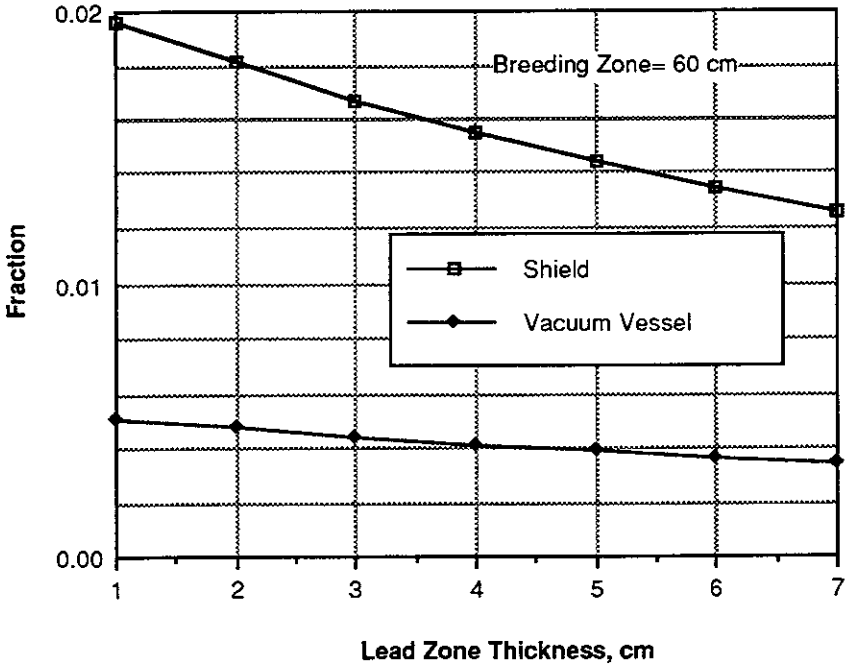

Figure 6.8.3-9. Fraction of Nuclear Power Deposited in the Vacuum Vessel and Shield Systems as a Function of Lead Zone Thickness

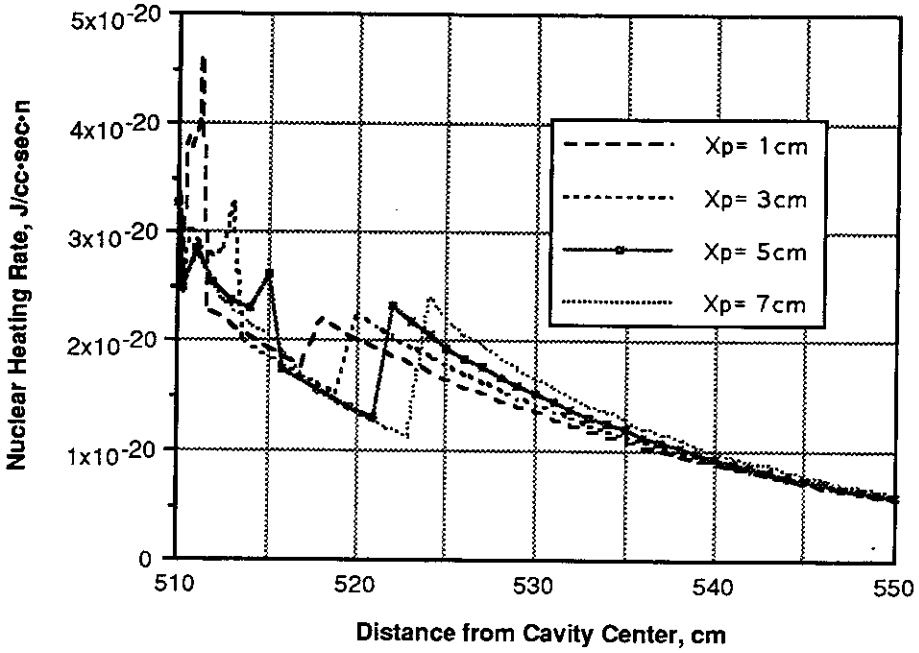

Figure 6.8.3-10. Nuclear Power Density as a Function of the Lead Zone Thickness

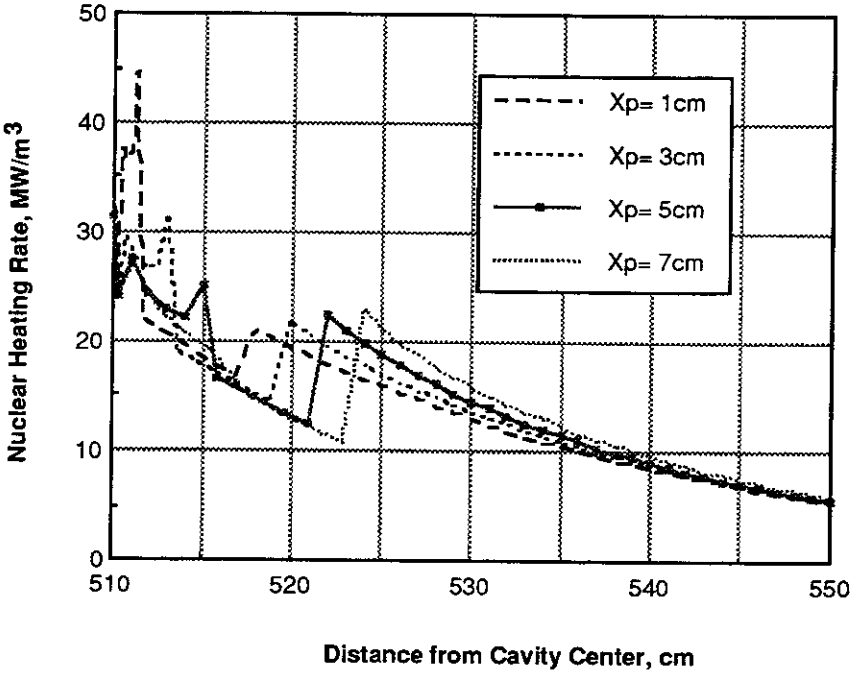

Figure 6.8.3-11. Nuclear Power Density as a Function of the Lead Zone Thickness

by neutron interactions with lead, particularly the inelastic scattering reactions (see Figure 6.8.1-3 in Section 6.8.1). The total nuclear heating rate in the first wall is ~24 MW/m^3 and is dominated by neutron heating (~75%). The average power density in the lead channel zone is ~25 MW/m^3, mainly from gamma ray heating (~80%). For the baseline case, the maximum heating rate in the breeding zone is ~20 MW/m^3 which occurs just behind the blanket first wall (2.5-cm thick, 84% SiC, 16% He). Nuclear heating in the breeding zone is attributed mainly to neutron interactions, particularly Li-6(n,α)T reactions.

The profiles for the tritium production rate (TPR) from Li-6 (T-6) are shown in Figure 6.8.3-12 as a function of Xp. By increasing the lead zone thickness, both neutron multiplication and inelastic collisions in lead increase, leading to larger TPR from Li-6 (and consequently a larger TBR) in approximately the first 30 cm in the breeding zone . This increase is more apparent just behind the first wall of the B/R/P system. For an increase in Xp from 1 cm to 7 cm, the local T-6 production rate is increased from 8.5x10^{-9} T atoms/cm^3•sec•n to 1.8x10^{-8} T atoms/cm^3•sec•n (a factor of 2.3 increase) at the front edge of the breeding zone. In the baseline case, this maximum local value is 1.5x10^{-8} T atoms/cm^3•sec•n.

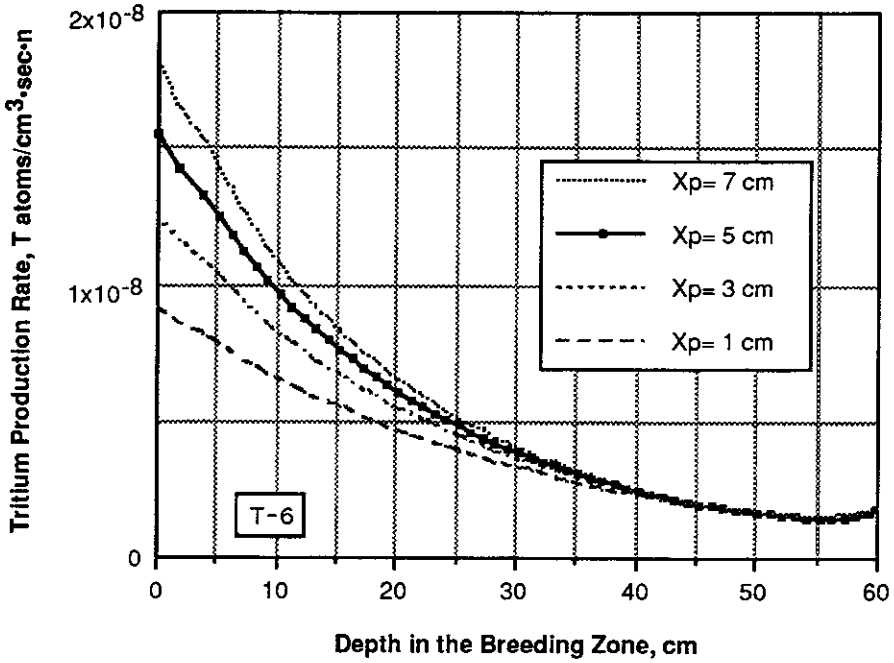

Figure 6.8.3-12. Tritium Production Rate From Li-6 (T-6) as a Function of Lead Zone Thickness

Figure 6.8.3-13 shows the corresponding profiles for the tritium production rate from Li-7 (T-7). By increasing lead in the FWS, the increase in the high-energy reactions in lead [e.g., (n,2n), inelastic] tends to decrease the tritium producing reactions in lithium-7, Li-7(n,n'α)T, whose threshold energy is ~2.8 MeV. However, the TPR from Li-7 is about an order of magnitude less than that from Li-6 behind the first wall of the blanket and, thus, increasing Xp leads to a net increase in the total TPR (and TBR). Note from Figures 6.8.3-12 and 6.8.3-13 that the profiles for T-7 are less steep than those for T-6 near the blanket first wall. The effect of increasing the lead zone thickness is less at the back locations in the breeding zone. In the baseline design (Xp = 5 cm), the TPRs from Li-6 and Li-7 are ~1.5×10^{-8} T/cm^3•sec•n and ~1.5×10^{-9} T/cm^3•sec•n, respectively, just behind the blanket first wall.

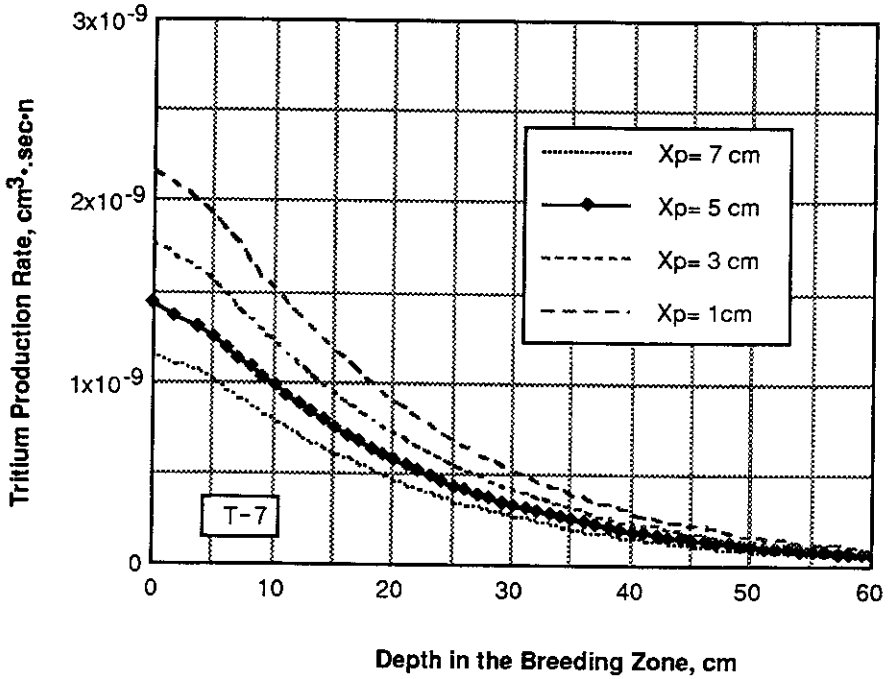

Figure 6.8.3-13. Tritium Production Rate from Li-7 (T-7) as a Function of Lead Zone Thickness

The impact of increasing the breeding zone thickness, X_B, on both M and TBR are shown in Figures 6.8.3-14 and 6.8.3-15, respectively. For Xp = 5 cm, the multiplication factor M slightly decreased upon increasing X_B while the TBR decreased. By increasing XB from 40 cm to 100 cm, M decreased from 1.146 to 1.131 (~2% decrease) while the TBR increased from 1.13 to 1.23 (~9% increase). The fraction of nuclear power deposited in the first wall system (~21%) is insensitive to this design change whereas the power deposited in the B/R/P system slightly increased from 0.74 to 0.79 (~7% increase). The fractions of power deposited in the various components are shown in Figures 6.8.3-16 and 6.8.3-17.

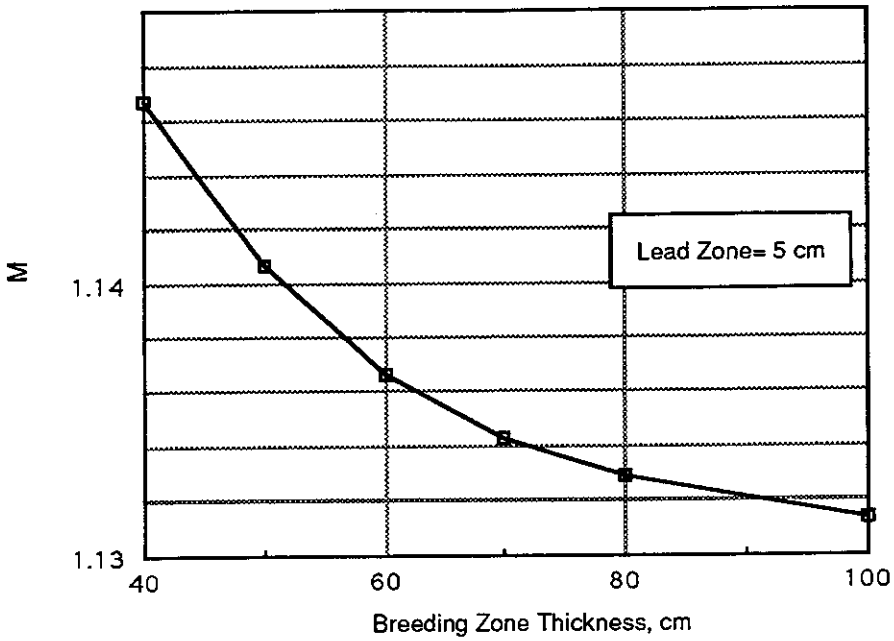

Figure 6.8.3-14. Nuclear Power Multiplication as a Function of the Breeding Zone Thickness

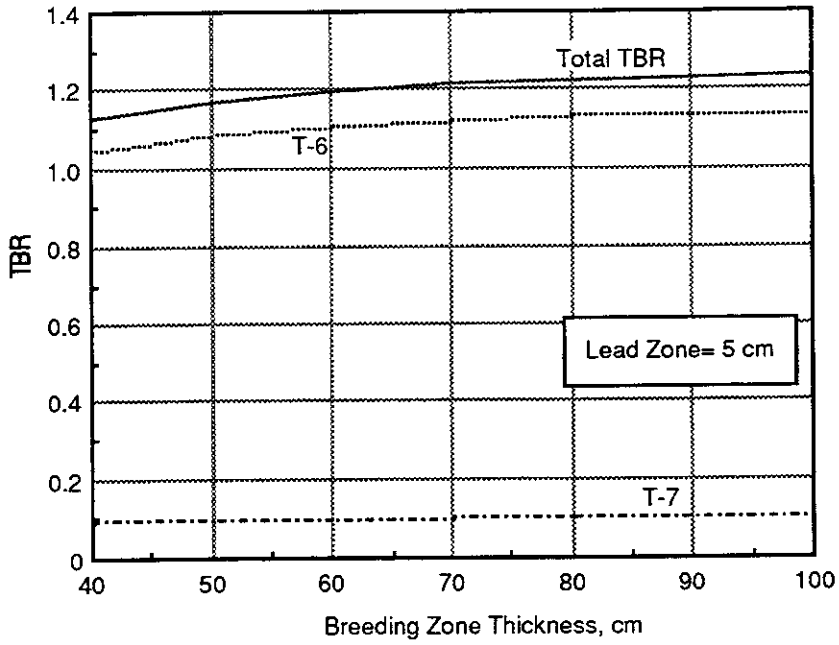

Figure 6.8.3-15. Tritium Breeding Ratio as a Function of the Breeding Zone Thickness

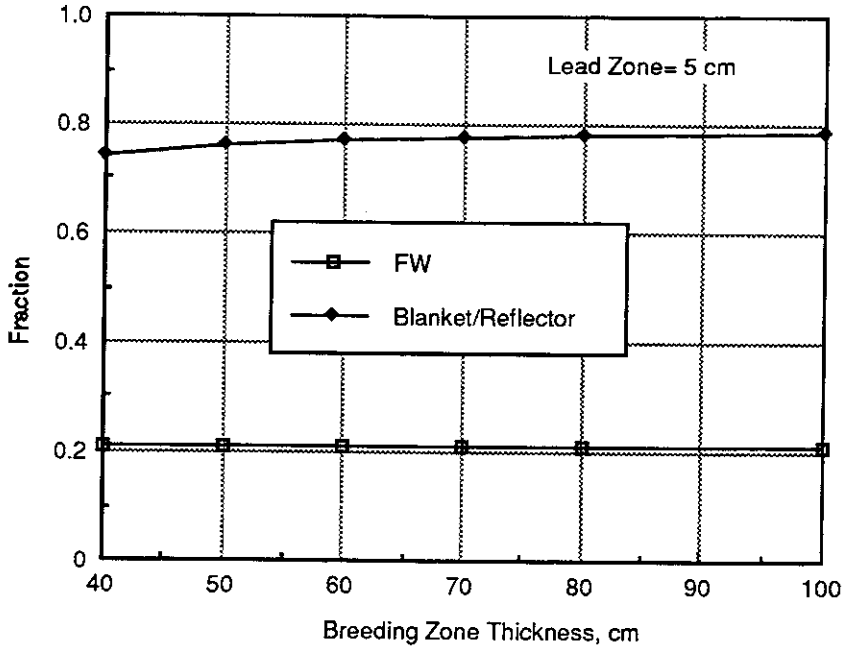

Figure 6.8.3-16. Fraction of Nuclear Power Deposited in the First Wall and Blanket/Reflector Systems

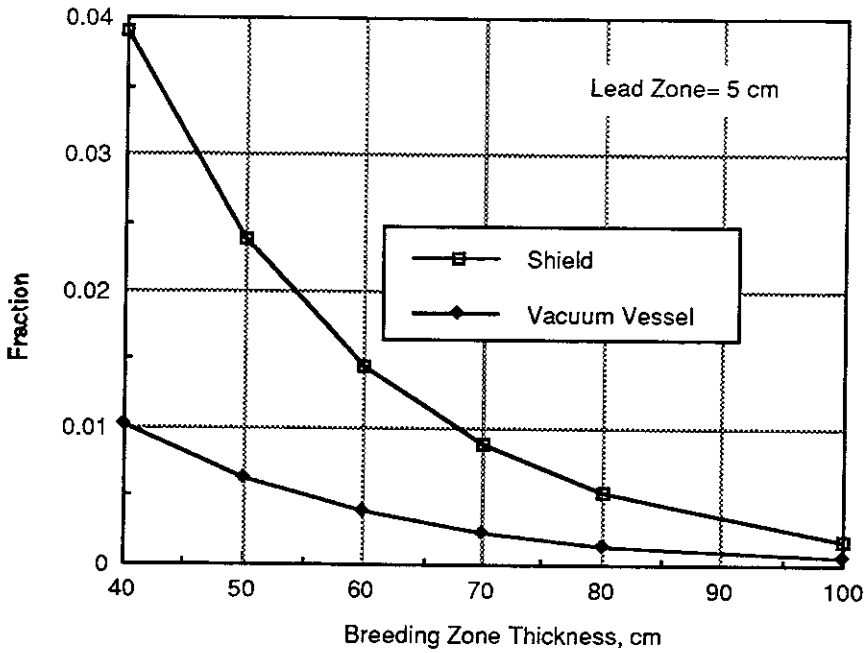

Figure 6.8.3-17. Fraction of Power Deposited in the Vacuum Vessel and Shield Systems

Nuclear Performance of the Baseline Design - From the above results, it was concluded that the nuclear power multiplication in our design is less sensitive to design variations than the TBR, which is most sensitive to the thickness of the Pb zone. The ^{6}Li-enrichment used in the parametric analyses was 25% which was determined to be optimal value in our design. In the baseline design, the Pb zone thickness and the breeding zone thickness are X_p = 5 cm and X_B = 60 cm, respectively. In this case, M ~ 1.14 and TBR ~ 1.2. The fractions of power deposited in the FWS, B/R/P, vacuum vessel, and the shield are 0.21, 0.77, 0.004, and 0.014, respectively. Table 6.8.1-2 in Section 6.8.1 lists these fractions (in %) by material zone as well as by system. The integrated power in each zone is expressed in terms of joules per incident source neutron and, thus, the entries do not depend on the fusion power, neutron yield, etc. To convert the entries given in Table 6.8.1-2 to absolute values (in MW), the following formula could be used:

(power deposited, J/n) • (incident neutron power, MW) • 4.85×10^{11}

or alternatively,

(% of power deposited, by zone) • (incident neutron power, MW) • 1.14

In the laser reactor design, the incident neutron power is 2027 MW while it is 1818 MW in the heavy ion reactor case. When the cavity power multiplication factor M=1.14 is applied, the nuclear power in the two reactors are 2311 MW and 2073 MW, respectively. Table 6.8.1-3 in Section 6.8.1 gives the cavity energy balance in the two reactors.

Effect of Including a Beryllium Zone on Blanket Characteristics – The nuclear characteristics of the reference blanket could noticeably be improved upon by incorporating beryllium in the blanket system. Several neutron transport calculations were performed in which the Li_2O in the first few centimeters of the breeding zone was replaced by beryllium (80% theoretical density). Figures 6.8.3-18 to 6.8.3-21 show the effect of this design change on the nuclear power multiplication, M, the tritium breeding ratio, TBR, and the power distribution in the FWS, B/R/P, vacuum vessel, and shield systems. With a beryllium zone thickness of 8 cm (i.e., replacing Li_2O in the first 8 cm in the 60-cm thick breeding zone with beryllium), the TBR increased from 1.198 to 1.279 (~7% increase) while M increased from 1.137 to 1.188 (~5% increase). This design variation could improve the COE and tritium fuel cycle.

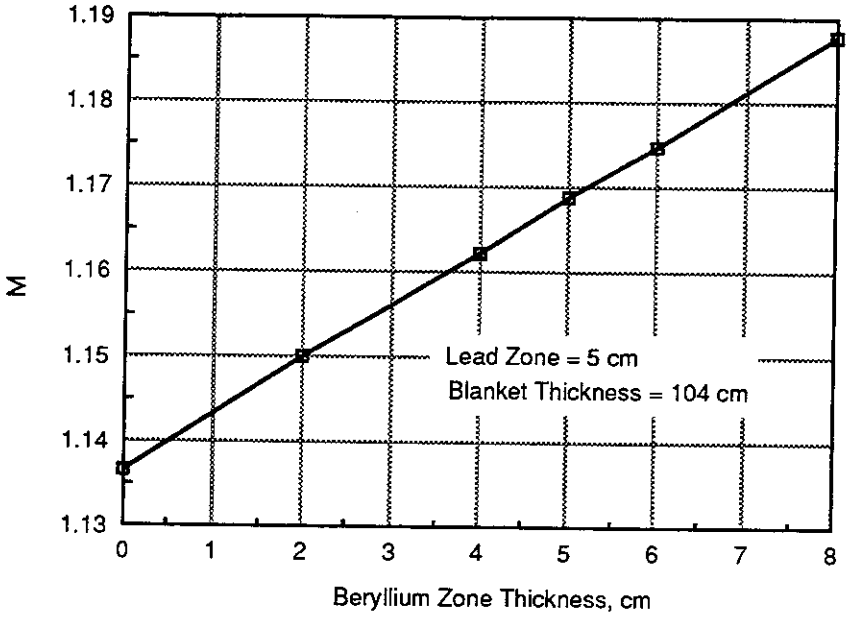

Figure 6.8.3-18. Nuclear Power Multiplication as a Function of the Beryllium Zone Thickness

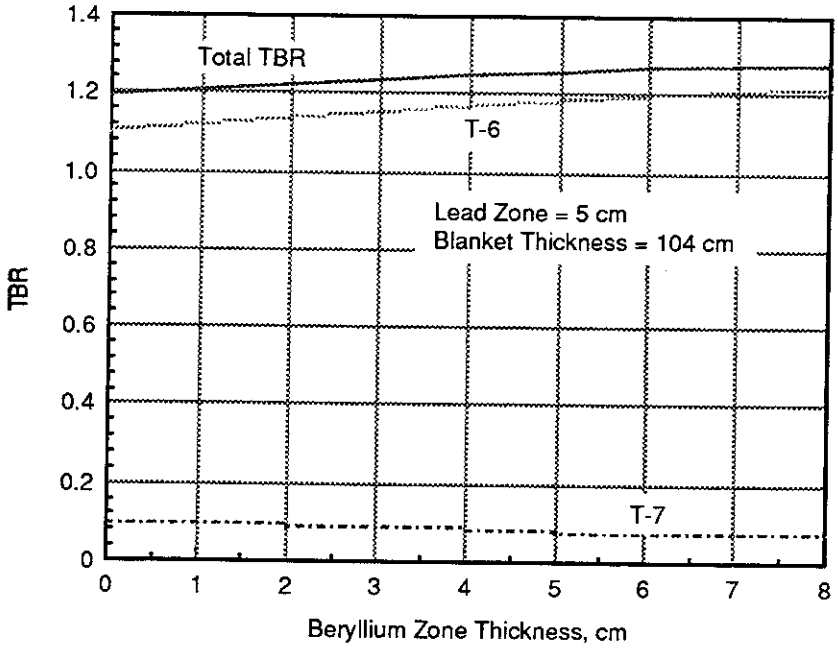

Figure 6.8.3-19. Tritium Breeding Ratio as a Function of Beryllium Zone Thickness

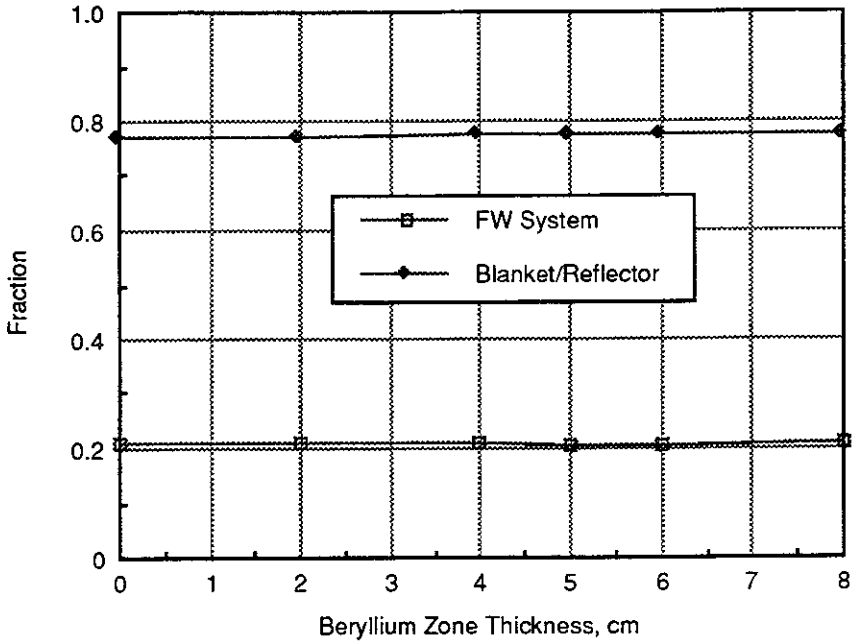

Figure 6.8.3-20. Fraction of Nuclear Power Deposited in the First Wall and Blanket/Reflector Systems as a Function of Beryllium Zone Thickness

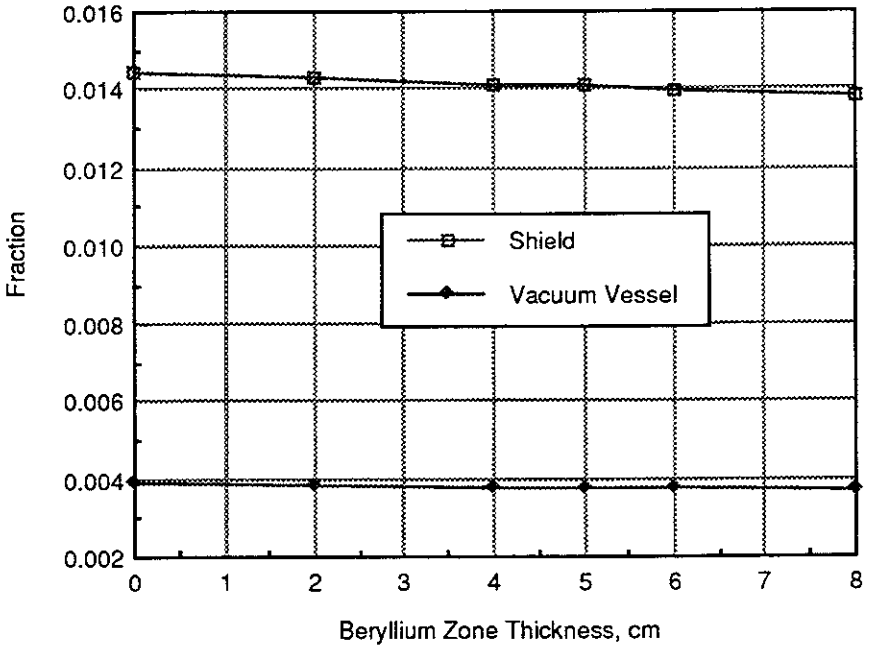

Figure 6.8.3-21. Fraction of Nuclear Power Deposited in the Vacuum Vessel and Shield Systems as a Function of Beryllium Zone Thickness

6.8.3.3 Thermal Hydraulics

Helium Coolant – The first wall protection system absorbs virtually all the energy from the x-rays and debris from the micro-explosion as well as a significant fraction of the neutron energy. This results in less than 60% of the total thermal power being deposited in the blanket, which opens the possibility of flowing the He at moderate pressure while keeping the pressure drop and velocity at reasonable levels.

A parametric study explored this possibility. The helium inlet temperature was set at 400°C to ensure that the solid breeder temperature would be higher. The outlet temperature was set at 650°C based on a tradeoff between maximizing the power conversion efficiency and the design simplicity. A high outlet temperature would result in higher power conversion efficiency whereas a lower outlet temperature would result in thicker breeder regions for the same breeder maximum temperature limit, and, thus, in fewer breeder layers per module and in a simpler design and assembly. Figure 6.8.3-22 shows the helium velocity as a function of the inlet pressure for different fractional flow areas for a temperature rise of 250°C and blanket power and total area of 1782 MW and 470 m^2, respectively.

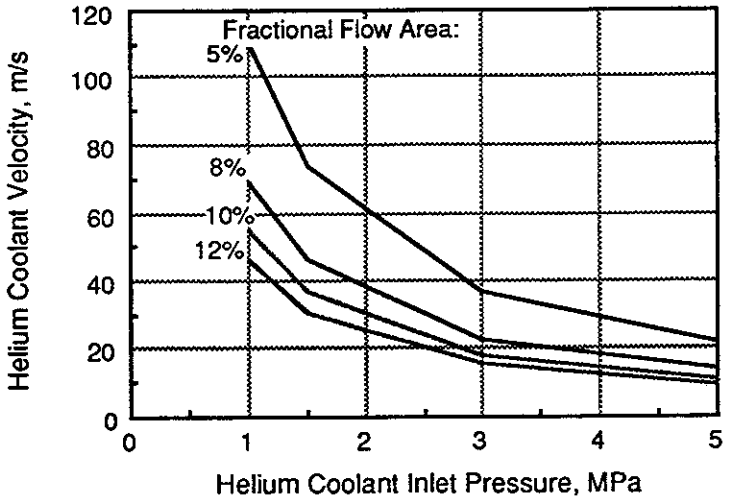

Figure 6.8.3-22. He Coolant Velocity in the Blanket as a Function of the Inlet Pressure for Different Fractional Flow Areas

The total He pressure drop in the blanket, ΔP_{tot}, was calculated as the sum of the pressure drops due to friction, ΔP_f, losses, ΔP_l, and acceleration, ΔP_a. The friction pressure drop component was calculated as follows:

$$\Delta P_f = \frac{fL}{d_H}\frac{\rho u^2}{2} \qquad (6.8.3\text{-}1)$$

where ρ is the density, u the velocity, L the flow length (~2 m), d_H the hydraulic diameter (~ 6 mm), and f the friction factor. For turbulent flow in smooth pipes, the friction factor can be estimated from the Reynolds number, Re, based on the Blasius equation:

$$f = 0.316\,Re^{-0.25} \qquad (6.8.3\text{-}2)$$

In addition, in the absence of specific data on the roughness of the SiC channels, a roughness factor of 2 was conservatively assumed in the calculation of the friction factor.

A value for ΔP_l was estimated from a loss coefficient, K, whose value was set at 3 based on assumed pressure losses through one expansion, one U-bend, and one constriction.

$$\Delta P_l = K\frac{\rho u^2}{2} \qquad (6.8.3\text{-}3)$$

Finally, ΔP_a was estimated based on the helium densities at the inlet and outlet.

$$\Delta P_a = \rho u^2\left(\frac{1}{\rho_{out}} - \frac{1}{\rho_{in}}\right) \qquad (6.8.3\text{-}4)$$

Figure 6.8.3-23 shows the total pressure drop in the blanket as a function of the fractional flow area for different inlet pressures and fixed inlet and outlet temperatures of 400°C and 650°C, respectively. For a fractional flow area of 8% (which corresponds to 16% of the total blanket area since space has to be provided for both inlet and outlet flows), the blanket pressure drop is only 24 kPa for an inlet pressure of 1.5 MPa. This is reasonable; however, the pressure drop in the cooling system outside the blanket could be quite high, leading to a lower overall cycle efficiency than would have been the case for a higher inlet pressure. This has to be evaluated against the improved reliability and safety associated with a moderate coolant pressure. In particular, a 1.5 MPa pressure provides the possibility of double containment of the coolant in the blanket. The possibility of using a moderate coolant pressure (1.5 MPa) is seen as being a distinctive feature for this blanket since previous designs made use of He at high pressure (5 MPa or more) and is chosen for the reference case. If operation at high pressure is shown to provide an acceptable level of reliability and safety, the blanket operating parameters can be changed accordingly for higher overall plant

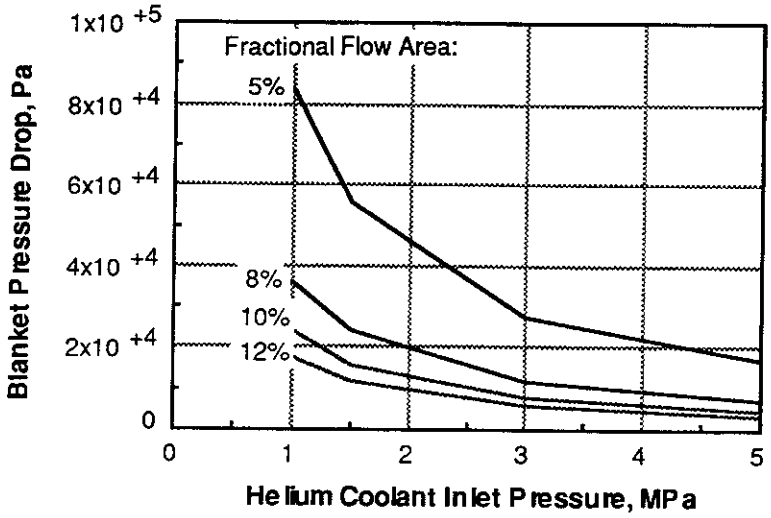

Figure 6.8.3-23. He Coolant Pressure Drop in the Blanket as a Function of the Inlet Pressure for Different Fractional Flow Areas. The Helium Temperature Rise is Fixed at 250°C

efficiency. From Figure 6.8.3-22, the corresponding velocity for an inlet pressure of 1.5 MPa is 46 m/s, resulting in a Re of about 6100.

Helium Purge - As shown in Figures 6.8.3-1 and 6.8.3-3, the purge flows in through an inlet manifold to the breeder regions. At the top of each breeder region at the inlet and outlet, a spacer acts like a plenum distributing the purge uniformly over the region at the inlet and guiding the purge to the manifold at the outlet. Orifices are placed in the inlet manifold so that, for the same pressure drop, the purge flow rate through each breeder region results in the same tritium partial pressure based on the tritium generation rate in the given region.

The packed bed form is selected for the breeder material instead of the sintered block form based mostly on perceived advantages in the accommodation of thermal expansion and swelling and in thermomechanical performance. In order to maximize the breeder volume fraction over the blanket region and, hence, the tritium breeding ratio, a binary Li_2O packed bed is chosen. The pebble sizes are 1.2 mm and 0.2 mm based on maintaining at least a ratio of 10 between the larger pebble size and the breeder region thickness (for better thermal performance predictability) and at least a ratio of 6 between the larger pebble size and the smaller pebble size (for better packing). The total Li_2O volume fraction in the breeder region is assumed to be 64%, which includes both the breeder theoretical density fraction (0.8) and the pebble bed packing fraction (0.8).

The purge pressure drop, ΔP_p, across the blanket region was estimated as a function of the pebble bed packing porosity, ε, and of the purge inlet pressure, $P_{p(in)}$ based on the Blake-Kozeny correlation for laminar flow (which is the regime of interest).

$$\frac{\Delta P_p}{L_b} = 150 \frac{(1-\varepsilon)^2 \mu V_0}{\varepsilon^3 d_{peff}} \qquad (6.8.3\text{-}5)$$

where L_b is the length of the breeder region over which the purge flows, μ is the fluid viscosity, V_0 the superficial velocity based on the total cross-section of the bed, and d_{peff} the effective particle diameter. V_0 can be estimated from the total mass flow rate of the helium purge, the helium density based on the inlet pressure and the total breeder region cross-section area. This area was estimated from a total blanket flow area of 235 m^2 and a breeder region area fraction of 0.55. The partial pressure of HT in the purge was set at 10 Pa based on tritium inventory considerations. For a tritium generation rate of 516 g/day (based on a fusion power of 2807 MW and a TBR of 1.2), the total purge mass flow rate is 1.61 kg/s. The value of d_{peff} is estimated by equating its reciprocal value to the summation of the ratio of weight fraction to diameter of each particle size. For a packed bed with 66% of particles of diameter 1.2 mm and 33% of particles with diameter 0.2 mm, d_{peff} is 0.45 mm.

Figure 6.8.3-24 shows the purge pressure drop per unit length in the blanket as a function of the bed packing fraction, (1-ε), for different purge inlet pressure and for an

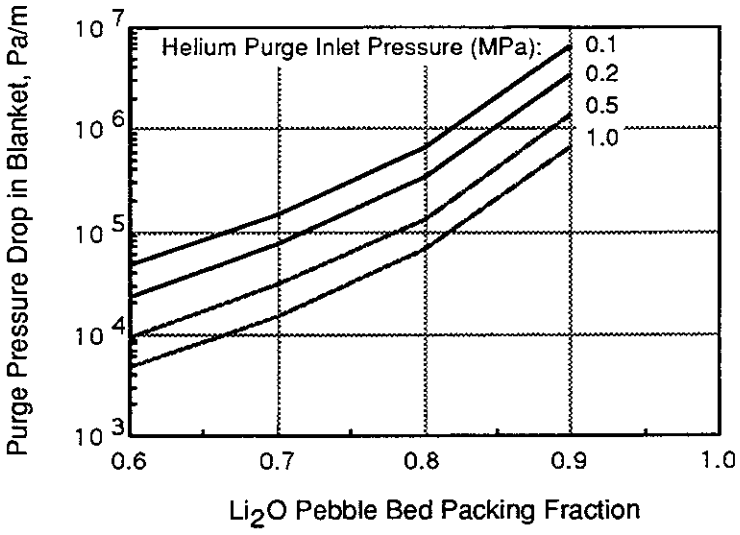

Figure 6.8.3-24. He Purge Pressure Drop in the Blanket as a Function of the Li_2O Bed Packing Fraction for Different Purge Inlet Pressures. The Flow Length Was Set at 2 m and the Effective Particle Size at 0.45 mm

average temperature of 700°C. The pressure drop is quite high and imposes a constraint on the choice of the purge inlet pressure. For example, for a packing fraction of about 0.8, a flow length of about 1.5 m and, assuming an arbitrarily set limit of 10% on the pressure drop to inlet pressure ratio, the required inlet pressure is about 1 MPa. This pressure is acceptable since it is lower than the coolant pressure (1.5 MPa), thereby preventing tritium contamination of the coolant in the case of a leak between the coolant and purge. Note that the pressure drop outside the blanket is relatively small and the total purge pressure drop will be set basically by the blanket pressure drop. The corresponding pumping power required for the purge is about 0.18 MW based on an assumed pump efficiency of 0.9.

6.8.3.4 Thermo-Mechanics – The moderate coolant pressure provides the possibility for each module to independently withstand the 1.5 MPa pressure in the unlikely event of a SiC tube sheet leaking or rupturing. This would be an added safety advantage, effectively resulting in double coolant pressure boundaries. To assess this possibility and to determine the required module dimensions, a simple stress analysis was carried out. The side wall thickness increases towards the back of the module to the same thickness of the back wall (see Figure 6.8.3-1) and stresses there can be more easily accommodated, in particularly since the thermal stresses are low. The stresses in the side walls toward the front of the module and the front walls are higher and more limiting and, thus, were the focus of the analysis.

Figure 6.8.3-25 shows a typical cross-section of the front wall. The total wall thickness is t_w, while the thickness of the SiC region on each side of the cooling tube region is t_h.

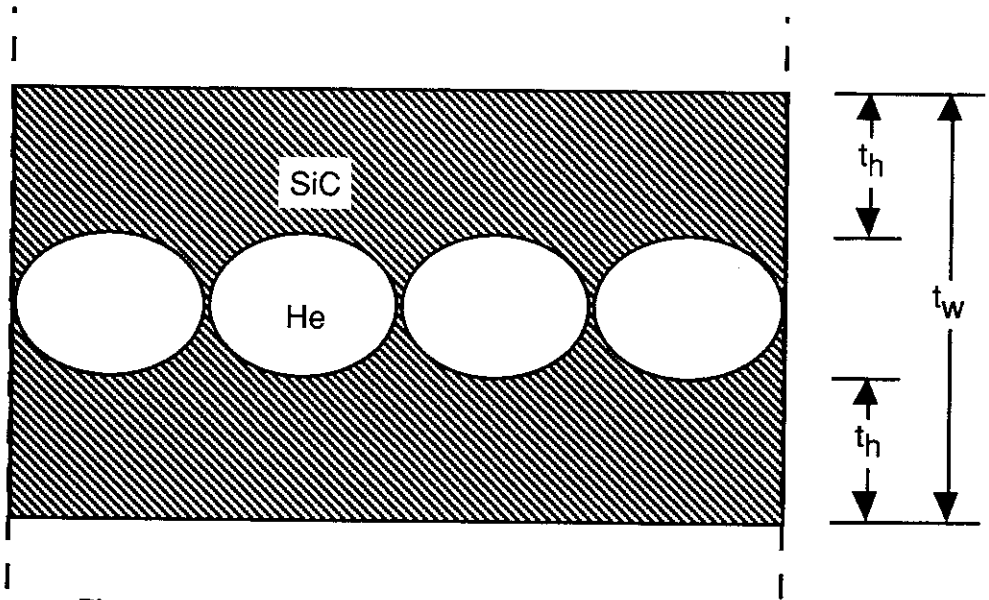

Figure 6.8.3-25. Cross-Section of the Module Front Wall Showing the He Cooling Channels

The thermal stress, σ_{th}, was first estimated based on the following expression:

$$\sigma_{th} = \frac{E\,\alpha\,\delta T}{2(1-\nu)} \qquad (6.8.3\text{-}6)$$

where E is Young's modulus of elasticity for SiC composite, α the coefficient of thermal expansion, and ν Poisson's ratio. δT is the temperature drop between the edge of the wall and the coolant channel which can be estimated from the distance, t_h, between the coolant channel and the wall edge, the heat generation per unit volume, q''', and the thermal conductivity of the SiC composite, k.

$$\delta T = \frac{q''' t_h^2}{2k} \qquad (6.8.3\text{-}7)$$

Figure 6.8.3-26 shows the thermal stress as a function of t_h for a q''' of 10 MW/m^3, typical of the front wall, and for the SiC composite properties listed in Table 6.8.3-2 based on those used in Reference 1.

Table 6.8.3-2. Properties of SiC Composite Used in the Stress Calculations

Young's Modulus of Elasticity, E	200 GPa
Coefficient of Thermal Expansion, α	4.5×10^{-6} K^{-1}
Thermal Conductivity, k	15 W/m-K
Poisson's Ratio, ν	0.18
Tensile Strength, S_T	200 MPa
Allowable Stress (assumed 2/3 S_T)	134 MPa

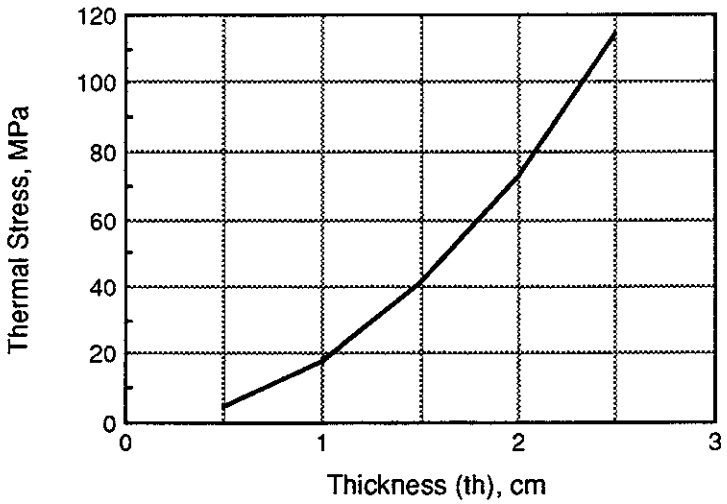

Figure 6.8.3-26. Thermal Stress in the Module Wall as a Function of the Distance Between the Coolant Channel and the Wall Edge

The bending stress was estimated by considering the module side walls and front wall (see Figures 6.8.3-1 and 6.8.3-3) as a series of plates with built-in edges of length 60 cm and width, w_r, set by the pitch between successive reinforcing ribs. The rounded corners linking the front wall to the side walls were considered separately and the stresses there were estimated using the simple hoop stress equation for a thin wall vessel.

From Reference 6, the maximum bending stress, σ_M, in a plate with built-in edges is given in terms of the maximum bending moment, M, and of the plate thickness, t_p.

$$\sigma_M = 6\frac{M}{t_p^2} \qquad (6.8.3\text{-}8)$$

For a plate with a length-to-width ratio greater than 2, the following expression is given in Reference 3 for M as a function of the pressure, P, and plate width, w_r (assuming a Poisson's ratio of 0.3):

$$M = 0.0833\, P\, w_r^2 \qquad (6.8.3\text{-}9)$$

Figure 6.8.3-27 summarizes the results. It shows the maximum bending stress in the plate as a function of the plate width for different plate thicknesses. From the results for a plate width of 0.25 m and thickness of 2 cm, the stress is 116 MPa. The plate thickness, t_p, here is assumed equivalent to 2 t_h from Figure 6.8.3-25. From Figure 6.8.3-26, the corresponding thermal stress is 18 MPA, resulting in a total stress of 134 MPa, which is acceptable. Thus, the wall thicknesses proposed for the reference case are t_w = 2.5 cm and t_h = 1 cm, and the proposed distance, w_r, between successive U-shape strengthening ribs along the length of the module is 25 cm. From the analysis, this set of dimensions would result in the module withstanding the 1.5 MPa coolant pressure in case of leak or failure. Development of SiC composite with higher tensile strength would provide more flexibility in setting these module wall dimensions.

The hoop stress in the rounded corners was estimated as being low, 15 MPa for t_p = 2 cm and for a pressure and radius of curvature of 1.5 MPa and 20 cm, respectively.

The results from the analysis are encouraging. However, in order to fully understand the stress behavior of the modules, an integrated 3-D analysis for the whole module is required which would take into account the effect of the ribs, the tapering wall thickness, and of the wall curvature in locations where space must be provided for beam penetration.

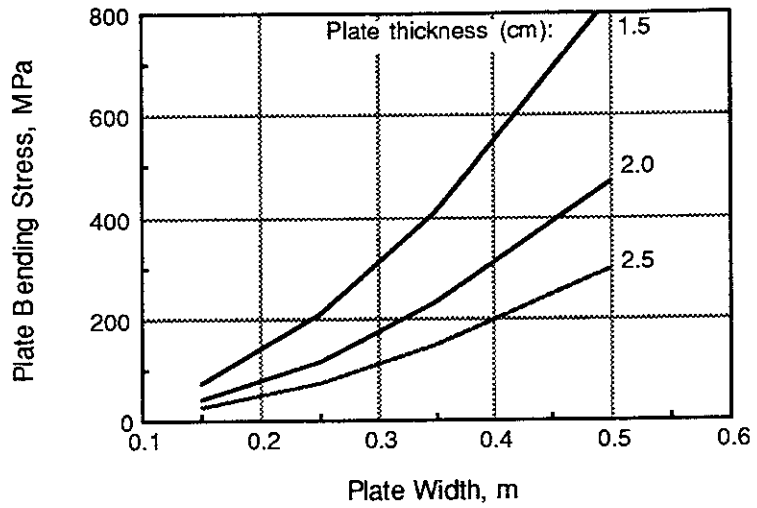

Figure 6.8.3-27. Maximum Bending Stress in a Plate with Built-In Edges as a Function of the Plate Width for Different Plate Thicknesses

6.8.3.5 Tritium Analysis - Accurate calculation of the tritium inventory in the Prometheus Li_2O blanket requires the knowledge of different properties, parameters, and conditions associated with the blanket. Unfortunately, many properties are not known for lithium ceramics. Therefore, an estimation can be made of the tritium inventory based on parametric studies and estimations of those missing data.

Calculations were made using the MISTRAL code.[7] This code includes the effects of the following transport processes:

(1) Diffusion of atomic tritium within the grain to the grain boundary.
(2) Diffusion of tritium along the grain boundary paths between adjacent grains to the solid/gas interface.
(3) Dissociative adsorption of gas species present in the pore onto the surface, "adsorption" of atomic tritium from the solid, surface recombination reactions, and associative desorption of tritium-bearing species to the pore.
(4) Diffusion of tritium-bearing species through the network of interconnected pores to the purge carrier.

In addition, a dissolution flux accounting for the return of some tritium atoms from the surface back to the bulk was also included in the code.

Assuming all other data is known and given, the tritium inventory will be mainly determined by the activation energy of solution and the heat of adsorption.[8] The activation energy of solution, E_s, is known for Li_2O. This energy was estimated by

Katsuta[9] as 16 kJ/mol for H_2 in Li_2O and 19 kJ/mol for D_2. For an HT mixture, Kudo and O'hira[10, 11] found E_s to be 24 - 25 kJ/mol.

The heat of adsorption, Q, is defined as

$$Q = E_{des} - E_{ads} \qquad (6.8.3\text{-}10)$$

where E_{des} is the activation energy of desorption and E_{ads} is the activation energy of adsorption.

The heat of adsorption is not known. However, although the adsorption energy is not known for most lithium ceramics, it is usually small for metals[12] and is between 3-15 kJ/mol for $LiAlO_2$, between 200 and 500°C.[13] Therefore, it can be safely assumed to be less than 25 kJ/mol. The activation energy of desorption was reported by several authors. For example, Bertone found E_{des} equal to 119 kJ/mol;[14] Miller, et al.[15] obtained a value between 125 and 140 kJ/mol from the CRITIC-I experiment; while Tanifuji [16] found E_{des} to be 148 ± 18 kJ/mol. Therefore, it is reasonable to assume the heat of adsorption in the range of 90-170 kJ/mol.

In estimating the tritium inventory, the effect of both the activation energy of solution and the heat of adsorption was examined. The effect of only these two energies was considered because the other energies are either known (such as the bulk diffusion activation energy) or do not have a significant effect on the inventory. Table 6.8.3-3 shows the input that was used in the code based on initial reactor and blanket parameters.

Table 6.8.3-3 Input Used in MISTRAL to Calculate the Blanket Tritium Inventory Results (See Figures 6.8.3-28 and 6.8.3-29)

Li_2O Theoretical Density Fraction	0.8
Li_2O Density (kg/m^3)	2.01×10^3
Helium Pressure (Pa)	2×10^5
Tritium Generation Rate (g/day)	362
Internal Surface Area of Porous Solid (m^2/kg)	50
Grain Radius (μm)	10
Maximum Temperature (°C)	800
Minimum Temperature (°C)	425
Amount of Protium in Purge (%)	0.2
Volume of Breeder Material (m^3)	92
Grain Diffusion Coefficient:	
Pre-exponential Factor (m^2/s)	6.81×10^{-7}
Activation Energy (kJ/mol)	84.8

Figure 6.8.3-28 shows the effect of the activation energy of solution on the tritium inventory at constant heat of adsorption (115 kJ/mol). The inventory decreases exponentially with increasing E_S in the range of concern (15-30 kJ/mol). This is consistent with Sievert's law which shows the solubility inventory to be proportional to $(\exp(-E_S/RT))$, where R is the universal gas constant and T is the temperature. For a given E_S, the solubility inventory would then increase exponentially with temperature, which has to be taken into account when setting the solid breeder operating temperature. Figure 6.8.3-29 shows the effect of the heat of adsorption on the tritium inventory at constant activation energy of solution (20 kJ/mol). The tritium inventory in this case has two distinct regimes. In the first region, the inventory is constant with Q. This is due to the fact that most of the inventory in this case is in the bulk, whereas Q affects mainly the surface inventory. In the second region, the surface inventory becomes dominant and, thus, the total tritium inventory increases exponentially with increasing the heat of adsorption.

From these two figures, a reasonable upper limit for the tritium inventory is 30 g, which corresponds to an activation energy of the solution of 15 kJ/mol and a heat of adsorption of 170 kJ/mol.

To reflect the latest reactor parameters, the tritium generation rate was increased to 516 g/day and the purge pressure to 1MPa and the resulting tritium inventory was still about 30 g. It should be noted, however, that these estimates do not include the effect of irradiation on the tritium transport which is not yet well characterized and still being studied. There is also a measure of uncertainty regarding the pre-exponential constants for the different surface fluxes, as reflected by the range of values obtained experimentally for the pre-exponential constant in the solubility expression for H_2 in Li_2O.

To account for unknowns, such as the irradiation effect, the proposed blanket inventory value is 100 g. This value corresponds to 0.5 wppm, which is of the same order as the results of EXOTIC 2 experiment ($\approx$ 0.1 and 1.5 wppm), CRITIC-I experiment ($\approx$0.6 wppm), and VOM 15H experiment ($\approx$0.7 wppm), which provide the only available measured inventory in irradiated Li_2O samples.[17] Note that these experiments were performed using materials with different microstructures and temperature levels, and that the Li_2O microstructure and the purge chemistry can be tailored for better tritium release.

A concern that needs to be addressed and better characterized is the effect of hydrogen in the purge on the SiC at high temperature. Reduction of the protective SiO_2 layer by hydrogen can result in formation of hydrocarbons and in loss of structural integrity of the SiC walls.

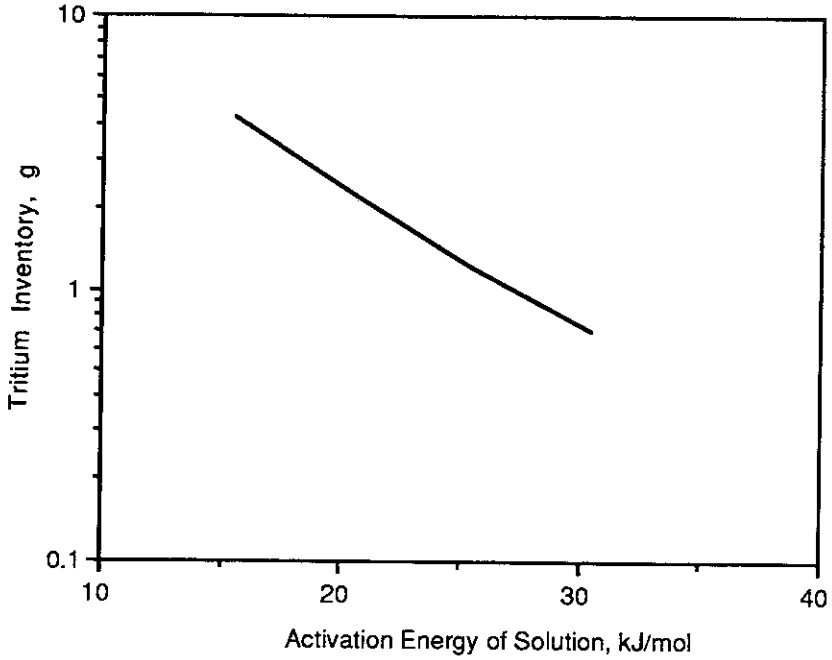

Figure 6.8.3-28. Tritium Inventory as a Function of the Activation Energy of Solution for Constant Heat of Adsorption (= 115 kJ/mol).

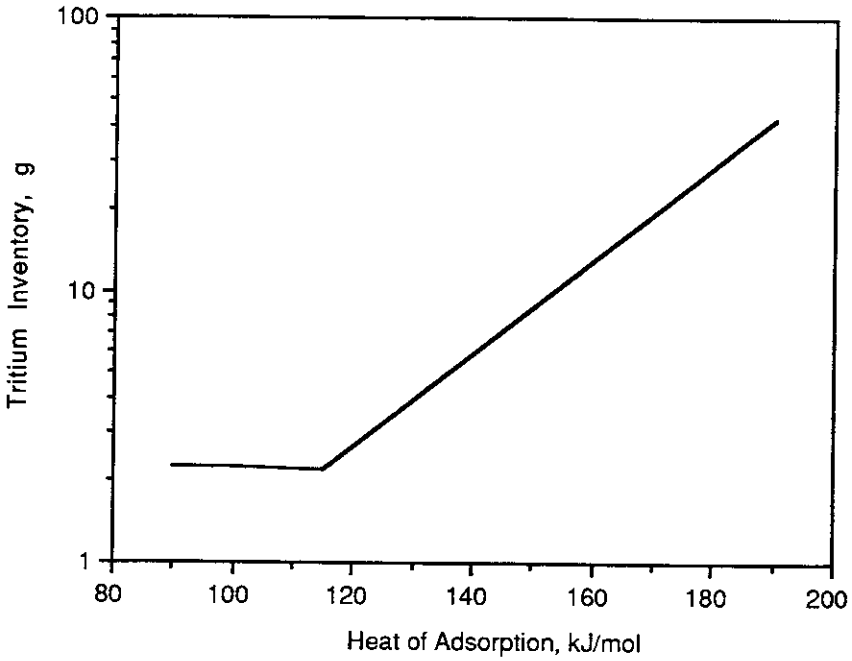

Figure 6.8.3-29 Tritium Inventory as a Function of the Heat of Adsorption for Constant Activation Energy of Solution (= 20 kJ/mol).

The tritium permeation through the SiC tube sheet wall from the purge to the coolant was also estimated based on a diffusion coefficient of 3×10^{-19} m^2/s at 600°C for β-SiC.[18] The tritium permeation flux was found to be negligible.

References for 6.8.3

1. F. Najmabadi, R. W. Conn, and the ARIES Team, "The ARIES-1 Tokamak Reactor Study," 16th Symposium on Fusion Technology, London, UK, 3-7 September 1990.

2. Y. Gohar, et al., "U.S. Technical Report for the ITER Blanket/Shield - A. Blanket," ITER-TN-BL-5-0-3, Garching, Germany, Section 3, July-November 1990.

3. B. Badger, et al.,"SIRIUS-M: A Symmetric Illumination, Internally Confined Direct Drive Material Test Facility," UWFDM-711, Fusion Technology Institute, University of Wisconsin, October 1986.

4. W. W. Engle, Jr.," A User's manual for ANISN," K-1693 (1967).

5. R.E. MacFarlane, " TRANSX-CTR: A Code for Interfacing MATXS Cross-Section Libraries to Nuclear Transport Codes for Fusion Systems Analysis," LA-9863-MS, Los Alamos National Laboratory, February 1984.

6. S. Timoshenko and S. Woinowsky-Krieger, "Theory of Plates and Shells," Second Edition, McGraw-Hill, New York, p197, 1959.

7. G. Federici, A. R. Raffray, and M. A. Abdou, "MISTRAL: A Comprehensive Model for Tritium Transport in Lithium-Base Ceramics – Part I and II," Journal of Nuclear Materials, 173, p. 184–228 (1990).

8. A Badawi and A.R. Raffray, "Analysis of Surface Fluxes of Hydrogen Species in Lithium Ceramics, "UCLA-FNT-50, December 1991.

9. H. Katsuta, S. Konishi and H. Yoshida, "Solubility and Diffusivity of Hydrogen in Li_2O, "Journal of Nuclear Materials, 116, p. 244-248 (1983).

10. S. O'hira, T. Hayashi, K. Okuno and H. Kudo, "Tritium Dissolution in and Release from Li_2O, " Fusion Eng. Design, 8, p. 335-338 (1989).

11. H. Kudo, K. Okuno and S. O'hira, "Tritium Release Behavior of Ceramic Breeder Candidates for Fusion Reactors," Journal of Nuclear Materials, 155-157, p. 524-528 (1988).

12. M.A. Pick and K. Sonnenberg, "A Model for Atomic Hydrogen-Metal Interactions - Application to Recycling, Recombination and Permeation," Journal of Nuclear Materials, 131, p. 208-220 (1985).

13. A.K. Fischer and C.E. Johnson, "Adsorption, Dissolution and Desorption Characteristics of $LiAlO_2$-H_2O(g) System," Semiannual Progress Report, DOE/ER-0313, p. 419-421, May 1989.

14. P.C. Bertone, "The Kinetics that govern the Release of Tritium from Neutron-Irradiated Lithium Oxide," Journal of Nuclear Materials, 151, p. 281-292 (1988).

15. J. M. Miller, R.A. Verrall, D.S. MacDonald and S.R. Bokwa, "The CRITIC-I Irradiation of Li2O - Tritium Release and Measurement," Fusion Technol., 14, p. 649-656 (1988).

16. T. Tanifuji, K. Noda, S. Nasu and K. Uchida, "Tritium Release from Neutron-Irradiated Li2O; Constant Rate Heating Measurements," Journal of Nuclear Materials, 95, p. 108-118 (1980).

17. M. C. Billone, "Modeling of Tritium Recovery from Lithium Ceramics," presented at the Second Workshop on Ceramic Breeder Interactions, Clearwater, Florida, 22-23 November 1991.

18. "Hydrogen Diffusion and Solubility in Silicon Carbide," Journal of American. Ceramic Society, p. 223, May-June 1978.